



Interface effect of graphene–TiO₂ photoanode with CuO nanorod counter electrode on solar conversion efficiency and enhanced external quantum efficiency

Bayram Kılıç¹

Received: 6 February 2019 / Accepted: 10 June 2019 / Published online: 14 June 2019
© Springer Science+Business Media, LLC, part of Springer Nature 2019

Abstract

In this study, graphene–TiO₂ nanostructures and CuO nanorods were produced on FTO (F:SnO₂) substrates using the cost effective hydrothermal growth method. The interface effects of the graphene–TiO₂ nanostructures were examined to compare with pure TiO₂ photoanode in respect to solar cell efficiency. Graphene–TiO₂ was shown as a perfect alternative for the standard F:SnO₂ (FTO)/TiO₂ working electrodes in dye-sensitized solar cells due to its higher electro-optic activity, surface area and good charge transport characteristics. Furthermore, CuO nanorods were also investigated as efficient counter electrodes (CEs) to be used in place of the conventional and costly platinum (Pt) CEs. By utilizing graphene–TiO₂ photoanode and CuO nanorod based CEs, hybrid solar cells with photovoltaic efficiency of 6.18% under AM 1.5G solar radiation were produced. According to the external quantum efficiency (EQE) of the hybrid solar cell agreement with the J–V measurements, the device based on the hybrid CuO CE exhibited higher EQE. EQE was improved by 30% compared to the Pt CE due to the higher J_{sc}, V_{oc} and the fill factor of the hybrid devices.

Keywords Graphene–TiO₂ · DSSCs · CuO counter electrode · Interface effect · Nano-semiconductors

1 Introduction

With the increase in the demand for new concept solar cells, dye sensitized solar cells (DSSCs) have attracted a great deal of interest due to their relatively high solar efficiency (up to 12%), easy design process and low material cost (O’regan and Grätzel 1991; Grätzel 2003). A standard DSSC includes four main components namely, titanium (IV) oxide

Electronic supplementary material The online version of this article (<https://doi.org/10.1007/s11082-019-1928-3>) contains supplementary material, which is available to authorized users.

✉ Bayram Kılıç
bkilic@yalova.edu.tr; kbayramkilic@gmail.com

¹ Department of Energy Systems Engineering, Faculty of Engineering, Yalova University, 77100 Yalova, Turkey

(TiO₂) based electrode or photoanode, Ruthenium based dye, I⁻/I₃⁻ electrolyte and platinum (Pt)/fluorine doped tin oxide (FTO) counter electrode (CE) (Hagfeldt et al. 2010). Photoanodes and CEs have a very important role in increasing solar cell efficiency in DSSCs. TiO₂ based photoanodes are used as nano-semiconductors and have been thoroughly studied due to their extraordinary optoelectronic properties (Chung et al. 2012). TiO₂ nanostructures with different crystal structures, such as anatase or rutile, show perfect solar cell efficiency as photoanode (Poudel and Qiao 2014; Mathew et al. 2014). Although TiO₂ nanostructures are commonly used in DSSCs, there are various issues that limit solar cell efficiency (Kakiage et al. 2015). For example, TiO₂ reduces photocatalytic effect due to its quick electron–hole recombination (Wang et al. 2008; Feng et al. 2008). In the present study, graphene based substrates were used in order to increase the performance of DSSCs, because graphene has a high surface area, reduces recombination rate and shows perfect electron transfer ratio. In addition, graphene has zero band-gap energy and exhibits a great potential that can be used for photovoltaic (PV) applications due to its excellent electron mobility at room temperature, high thermal conductivity and superior optoelectronic properties (Golobostanfard and Abdizadeh 2014; Zhang and Cao 2011). CEs also have a very important role in increasing cell efficiency in DSSCs. In standard DSSCs, Pt is applied as CE because of its perfect conductivity (Qin et al. 2010). Although Pt exhibits a high performance, Pt sources are difficult to find and scarce Pt materials lead to high costing DSSCs (Odobel and Pellegrin 2013; Morandeira et al. 2008). In this study, copper(II) oxide (CuO) nanorods were used as substitutes for Pt in the CE part of the DSSCs. CuO has a narrow band-gap energy between 1.2 and 2 eV and a wide absorption band in the visible region. In addition, CuO is composed of abundant and non-toxic materials and can easily be produced at a very low cost. Due to the aforementioned reasons, CuO is an appealing material for various applications (Anandan et al. 2005a). Depending on the annealing temperature and molar ratio, CuO can be produced in two composites, namely cuprous oxide (Cu₂O) and cupric oxide (CuO). CuO shows a cubic crystal structure and it has been shown that CuO is among the suitable candidates to be used in PV applications because of its perfect material properties (Favereau et al. 2013; Wood et al. 2014; Le Pleux et al. 2011). Choi et al. focused on systematic studies of dissolution engineering for Pt_{0.9} M_{0.1}/graphene (M = Au, Co, Cu, Fe, Mo, Ni, Pd, Ru, and Sn) CEs. The nanohybrid materials they developed exhibited higher catalytic activity and electrical conductivity compared to Pt/graphene CEs (Dao et al. 2017). In another study, they carried out the first synthesis of FeNi/RGO using DPR and suggested it as an alternative CE for DSSCs. They reported that iron-nickel-reduced graphene oxide (FeNi/RGO) exhibited ultrahigh catalytic activity, good conductivity and long-term stability for the reduction of triiodide (I₃⁻) ions in the CEs in the DSSCs (Sim et al. 2018). In order to explore cost-effective and efficient Pt-free CEs, Dao et al. presented the synthesis of a new type of cobalt nickel (CoNi) alloy on an RGO-coated FTO CE for DSSC applications using the DPR method. They determined that the highest efficiency was 6.75% for the device using Co_{0.3}Ni_{0.7}/RGO CE, which was higher than those of the devices using Pt CE (6.63%), Co/RGO (6.33%) and Ni/RGO (5.52%) (Park et al. 2017). As a new CE, cost-efficient cobalt palladium (CoPd) alloy/reduced RGO CEs were used in order to increase solar cell efficiency (Oh et al. 2017). They also determined that the cells using Co/RGO and Pd/RGO exhibited efficiencies of 5.17% and 5.41%, respectively.

In the present study, graphene–TiO₂ nanostructures were used as photoanodes in DSSCs. The high solar conversion efficiency of the graphene–TiO₂ nanostructures in the applications of DSSCs requires a proper design that decreases high photon absorption and electron loss during the excitation state. It was determined that the properties of the graphene–TiO₂ nanostructures depend on the nature of the production method and that the

role of the optimum experimental parameters improves the N719 dye loading and decreases the charge recombination. Different from the studies in the literature, this study used graphene–TiO₂ photoanodes with CuO nanorods for CE for the first time and produced a cell with an efficiency of 6.18% under AM 1.5G solar radiation. These results clearly show that high efficient solar cells can be produced by using both graphene/TiO₂ photoanodes and CuO CEs.

2 Experimental

For the preparation of the nanoporous graphene–TiO₂ based photoanodes, F:SnO₂ (FTO) substrate was cleaned with acetone, methanol, trichloroethylene and deionized water (DI), respectively. The RGO was prepared in accordance with the Hummers method (Dao et al. 2017). The RGO was coated onto the FTO substrate using dip-coating method. The graphene coated FTO substrate was examined by using X-ray powder diffraction (XRD) and Raman spectra analyses. As can be seen from the Supplementary Information (SI 1), the XRD and Raman measurements confirmed that pure graphene nanostructures can be successfully produced on FTO substrates. A solution of 1 mM TiO₂, 20 mL of hydrogen chloride (HCl), and 50 mL DI water were put into a Teflon lined autoclave. 8 mL of an ammonia solution was blended into the solution to adjust the pH level to 10.50. The FTO substrates were placed into the solution and the autoclave was heated to 180 °C for 12 h. After the hydrothermal growth, the graphene based TiO₂ nanostructures were annealed at 300 °C in air for 30 min to produce the photoanode (Fig. 1).

The CuO nanostructures were also produced to be used as CEs in DSSCs on the FTO substrate using the hydrothermal method. 0.5 g CuCl₂ + 2H₂O and 50 mL DI water were prepared and added into an autoclave. An ammonia solution was added into the solution to adjust pH of the solution to 9. CuO nanorods were obtained on FTO substrates after 16 h at 180 °C. To assemble a DSSC, complex N719 dye were used on the graphene based TiO₂ nanostructure photoanode. The graphene–TiO₂ nanostructures were immersed into the N719 solution for 6 h to adsorb the dye and the graphene/TiO₂/N719 was washed with ethanol two or three times. I⁻/I₃⁻ electrolyte were injected between the photoanode and CE,

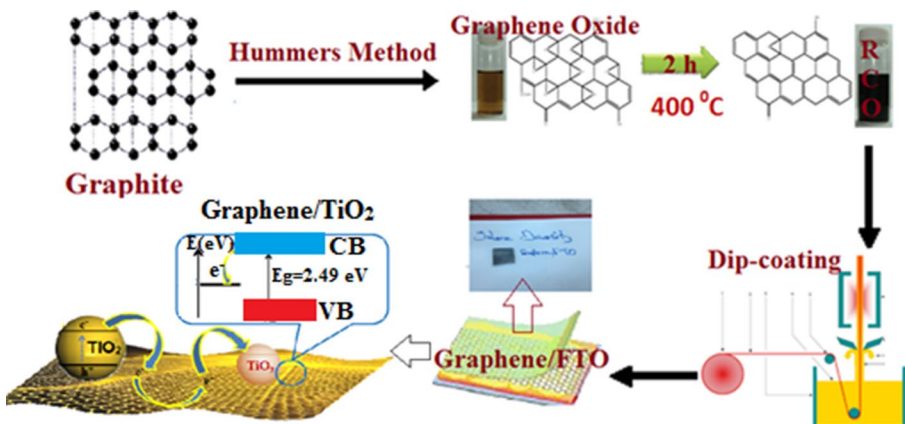


Fig. 1 Production mechanism of graphene–TiO₂ nanostructures

and solar cells were obtained with two different CEs. The Pt/FTO and CuO covered FTO CEs were used to compare the performance of the solar cells in terms of solar conversion efficiency.

3 Results and discussion

The scanning electron microscopy (SEM) images and the results of XRD, Raman, atomic force microscopy (AFM) and UV–Vis spectra of the graphene–TiO₂ nanostructures are exhibited in Fig. 2a–d. The SEM images in Fig. 2a, b show that the TiO₂ nanostructures were produced on graphene based FTO substrates with a nanoporous diameter of 20–50 nm. The cross-section of the SEM images indicates that graphene–TiO₂ nanostructures can be obtained at approximately 9.99 μm film thickness (Fig. 2b). The XRD analysis shows strong diffraction peaks which indicate that the graphene–TiO₂ nanostructures can be obtained with high crystal quality (inset in Fig. 2a). The Raman spectra shows three peaks at 418, 541 and 660 cm^{-1} related to the Raman active modes of TiO₂ nanostructures. The Raman peaks at 1414 and 1520 cm^{-1} show the standard D and G bands of the graphene (Fig. 2c). Choi et al. confirmed that garphene nanosheets had a similar band spectrum in D band spectrum can be fit using only a single peak centered at 1357 cm^{-1} . G and bands are centered at 1587 cm^{-1} and 1620 cm^{-1} (Dao et al. 2014). The AFM and UV–Vis spectra of the graphene–TiO₂ nanostructures are given together in Fig. 2d. In addition to

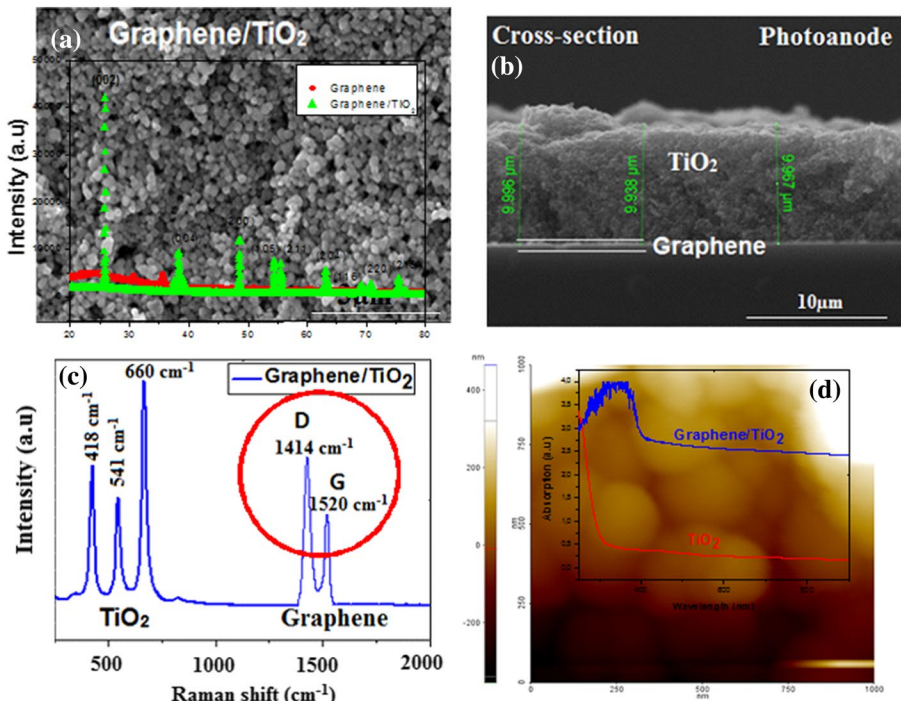


Fig. 2 a SEM and XRD characterization of graphene–TiO₂ nanostructures, b cross-section SEM images, c Raman, d AFM and UV–Vis spectra characterization of graphene–TiO₂ nanostructures

the SEM measurements, the surface morphology of graphene-TiO₂ was also investigated with contact mode AFM. The AFM measurements showed that the excellent surface structures of TiO₂ were obtained on graphene and provided clearer information about the surface properties. In addition, the AFM measurements also showed that the graphene-TiO₂ nanostructures were obtained as approximately 20–40 nm by homogeneously being distributed on the substrate in a three-dimensional (3D) view. The UV-Vis absorption spectrum is shown in the inset of the AFM in Fig. 2d. The absorption spectrum of the graphene-TiO₂ nanostructures shows strong absorption around 320 nm. Therefore, it was determined that the interactions between graphene and TiO₂ can lead to a narrow band-gap and enhanced visible light absorption. The band-gap energy of the graphene-TiO₂ nanostructures was obtained as 2.49 eV from the Tauc plot [The figure is shown in the Supplementary Information (SI 2)].

The fourier transform infrared spectrophotometry (FTIR) spectra of the graphene-TiO₂ nanostructures are exhibited in Fig. 3a. The FTIR spectra showed absorption bands at 650 and 1200 cm⁻¹, indicating the presence of a Ti-O-Ti bond in the TiO₂ nanostructures. The absorption peaks were 1218 cm⁻¹ for C-O stretching, 1220 cm⁻¹ for C-OH bond and 1364 and 1748 cm⁻¹ for the -OH groups of water molecule and C=O stretching, respectively. However, it can be indicated that the absorption spectra which was centered at 2973 and 3500 cm⁻¹ is based on the O-H groups of graphene. A photoluminescence (PL) spectra was carried out to investigate the recombination of the electron-hole pairs in the

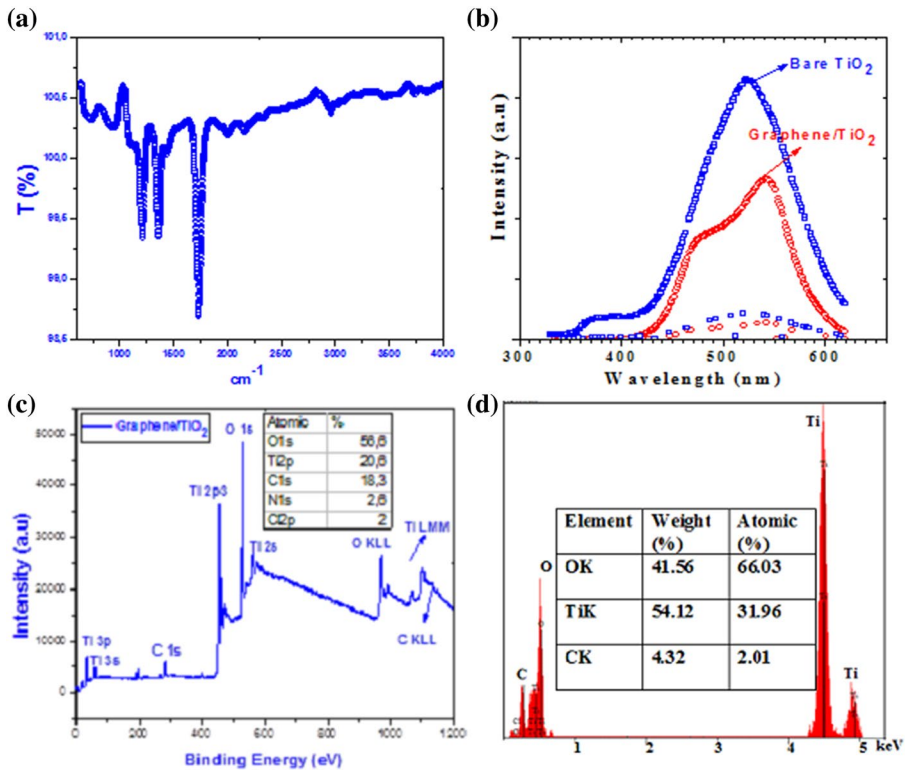


Fig. 3 a FT-IR, b PL, c XPS, d EDX characterization of graphene-TiO₂ nanostructures

graphene–TiO₂ nanostructures. The PL spectrum detected the recombination efficiency of the electron–hole pairs. The PL measurements of the graphene–TiO₂ nanostructures were much lower than those of the bare TiO₂ due to the electron–hole recombination (Fig. 3b). The PL spectra indicated that the photo-induced electron and hole were excited on the conduction band (CB) and valence band (VB) of TiO₂, respectively. The electrons in the CB of TiO₂ were moved onto the graphene. The Fermi level position between the graphene and TiO₂ nanostructures prevented the direct recombination of electrons and holes. In addition, the hybrid structures of the graphene–TiO₂ nanostructures may define the quick absorption sites for the photo-induced electrons and holes due to the band-gap alignment of their CB and VB. X-ray photoelectron spectroscopy (XPS) characterizations were carried out to investigate the interactions between the two components in the hybrid structures. The XPS spectrum of the graphene–TiO₂ gave the photoelectron peaks of titanium (Ti), oxygen (O), and carbon (C), confirming the existence of graphene and TiO₂ hybrid structures (Fig. 3c). The chemical characterization of the graphene–TiO₂ nanostructures was examined by energy-dispersive X-ray spectroscopy (EDS). The EDS measurements of the graphene–TiO₂ hybrid structures are shown in Fig. 3d. The EDS measurements demonstrated the presence of the Ti, O and C peaks. The results indicated that graphene–TiO₂ hybrid structures with a homogenous distribution can be produced.

The SEM image in Fig. 4a, b shows the spherical surface morphology of the CuO nanorods. It is indicated that CuO nanorods can be produced on the FTO substrate. The homogeneous distribution of the uniformly produced CuO nanorods on the substrate gave high electrical conduction pathway. The cross-section of the SEM image shows that the film thickness was around 30 μm . The radius and length of the nanorods were 50 nm and 2.50 μm , respectively. In order to study the stoichiometry of the samples, quantitative analysis was carried out using EDS. The EDS spectra of the CuO nanorods are shown in Fig. 4c in which it can clearly be seen that the materials were composed of O and copper (Cu). The XRD characterization of the CuO nanorods is shown in Fig. 4d in which they exhibit strong diffraction peaks at 32.8°, 35.9°, 39.2°, 48.8° and 61.9° degree 2 θ . These peaks come from the diffraction lines of the (110), (-111), (200), (-202) and (-113) planes of the monoclinic CuO structure (JCPDS No. 05-0661). This result confirms that high purity of the CuO nanostructures can be obtained on the respective substrates. The crystallite size was found to be approximately ~ 30 nm, which was in compliance with the XRD studies. Figure 4e indicates the UV–Vis spectra of the CuO structures prepared with 28% ammonia solution and annealed at 300 °C. The UV–Vis spectra show that the CuO structures had a wide absorption spectrum between 300 and 800 nm. Figure 4e shows the plot of $(\alpha h\nu)^2$ versus photon energy which is used to calculate the bandgap energy of the CuO nanostructures. The results showed that the structures had a narrow band-gap energy (E_g) of 1.56 eV.

The J–V characterization and external quantum efficiency (EQE) with schematic of graphene–TiO₂ and CuO CE taken under AM 1.5G solar irradiation are exhibited in Fig. 5a, b. To confirm the effect of graphene in the hybrid materials for photoanodes, current density–voltage characterization of the pure TiO₂ photoanode was also given (J–V characterization is shown in Supplementary Information (SI 3)). The current density–voltage characterization showed that when pure TiO₂ photoanode was used with Pt and CuO CE, solar conversion efficiencies were obtained as 2.51% and 3.18%, respectively. When the graphene based TiO₂ photoanode was used with CuO CE instead of Pt CE, the solar conversion efficiency (η) of the DSSC was improved by 30% and reached 6.18%. The improvement of solar conversion efficiency is mainly a result of the rapid inter conversion between liquid electrolyte, the possible back reflection of incident photons from the CuO CE layer

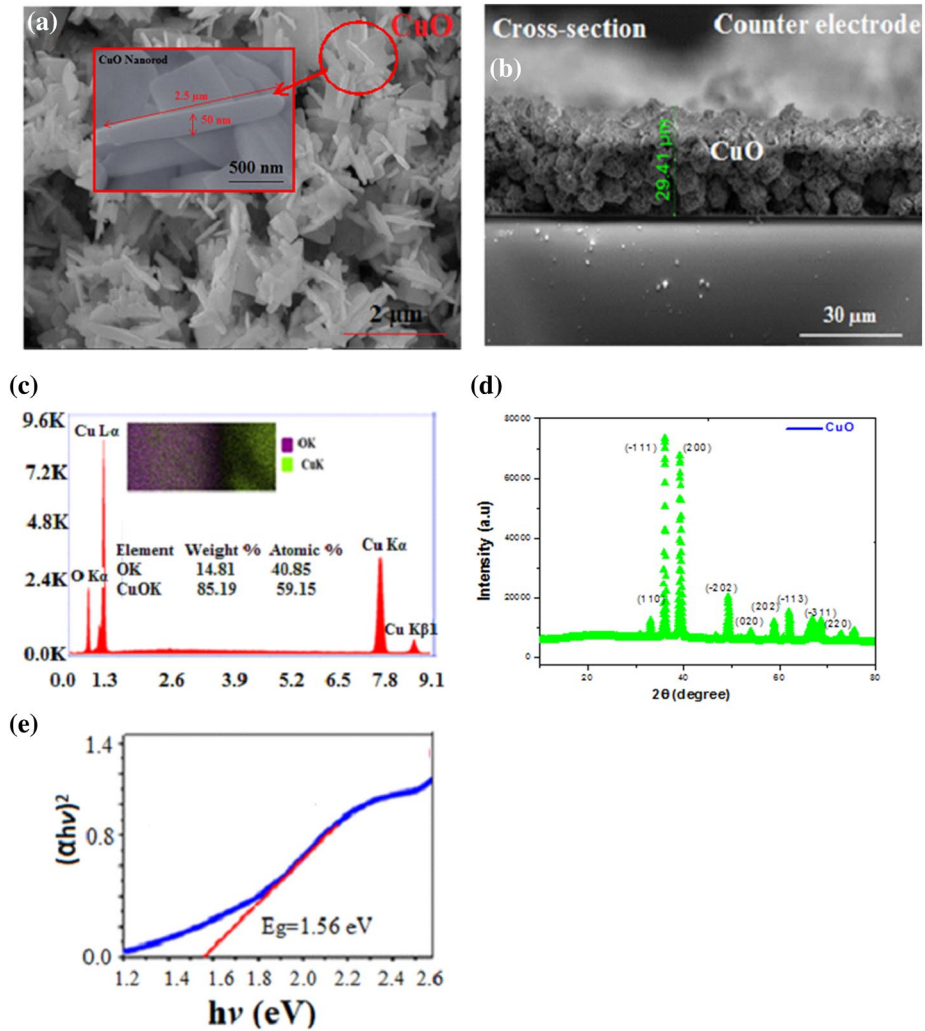


Fig. 4 **a, b** Top-view and cross-section SEM images, **c** EDX, **d** XRD, **e** UV–Vis spectra characterization of CuO nanorods

and the absorption of some photons by the CuO structures. Solar cell parameters such as J_{sc} , V_{oc} , FF and the corresponding solar cell efficiency values (η) of each cell are summarized in Table 1. The devices composed of four main components: graphene based on wide band-gap nano semiconductors as photoanode, N719 dye molecules, I^-/I_3^- liquid electrode, and a CuO nanowire as CE placed on the top of the semiconductors (inset Fig. 5b). When the devices came into contact with solar light, the electrons were excited from the highest occupied molecule orbital (HUMO) to the lowest unoccupied molecular orbital (LUMO) in the adsorbed dyes, then moved into the CB of TiO₂ and finally diffused in the TiO₂ to the graphene–FTO interface, where they were extracted to an external load. The depleted dye was reproduced by iodine (I), and the generated I₃ ions diffused to the CuO CE where the I₃ was reduced back to I. Compared with Pt CE, the CuO nanorods provided higher solar cell

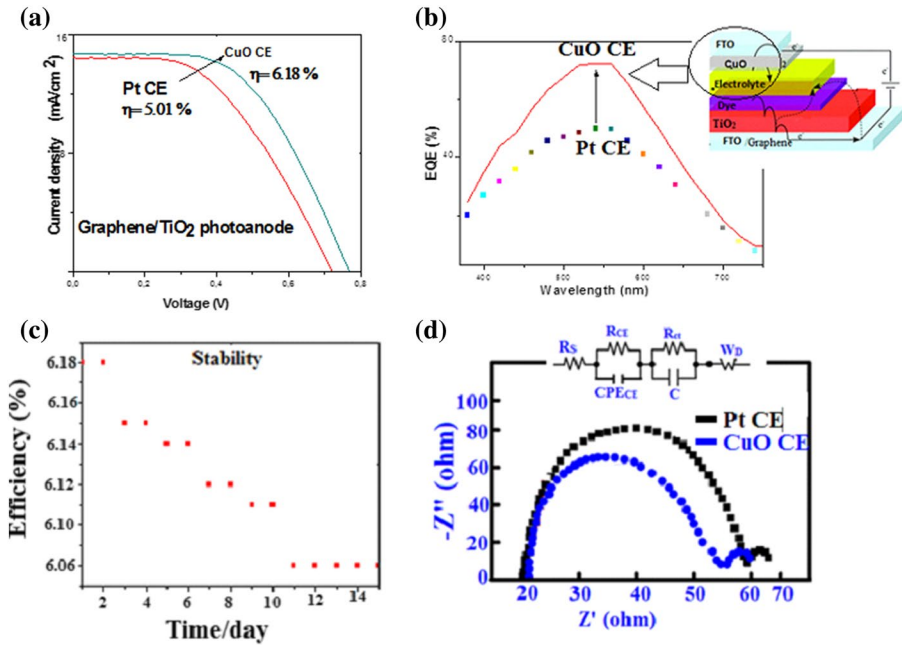


Fig. 5 **a** J–V curves of the two different counter electrode in DSSCs, **b** EQE of graphene–TiO₂ nanostructures–CuO counter electrode with schematic illustration of devices, **c** stability test of the solar cell, **d** EIS characterization of CuO and Pt CE in DSSC with the equivalent circuit model

Table 1 Photovoltaic properties of the graphene–TiO₂ photoanode with CuO CE

Sample	FF (%)	Voc (V)	Jsc (mA/cm ²)	η (%)
Pt CE	48.6	0.71	14.47	5.01
CuO CE	54.8	0.76	14.76	6.18

Measurements were performed under AM 1.5G one sun (light intensity: 100 mW cm⁻²). For all the cells, the active area was set at 0.25 cm²

efficiency, Voc, Jsc, and FF. Anandan et al. (2005b) first demonstrated vertically aligned CuO nanorod arrays produced on a Cu electrode to be applied as a CE in TiO₂ photoanode based DSSCs. They obtained a power conversion efficiency ranging from 0.12 to 0.29%. Tsai et al. (2018) indicated that when CuO was used as the CEs, the device conversion efficiency was 2.73%. They explained that CuO is a suitable replacement for Pt as it has a simple production method and is cheap and abundant. Sharma et al. (2015) demonstrated that a high solar-to-electrical energy conversion efficiency of η=3.4% was recorded in the DSSC produced with synthesized CuO nanoparticles (NPs) based CE. Liu et al. (2007) presented a solar cell efficiency result of η=1.12% for CuO nanoneedle array prepared on a pure Cu NC line layer by thermal oxidation in air for application as a CE in TiO₂-based DSSCs. In the present study, the external quantum efficiency was carried out from 350 to 900 nm in order to investigate the behavior of the graphene/TiO₂ photoanode with CuO CE in a wider spectral range. The results (Fig. 5b) indicate that the EQE in the near-ultraviolet range clearly improved with Pt CE. It was shown that the quantum efficiency increased when the

CuO nanorods were used as CE instead of Pt CE. The EQE measurements demonstrated an increase of quantum efficiency which is an indication of the extra electrons produced in the hybrid devices. In agreement with the J–V measurements, the device based on the hybrid CuO CE exhibited higher EQE. It was shown that the CuO nanorods had a perfect photocatalytic effect and a huge potential for CE applications in DSSCs. This study investigated the performance and stability of CuO based CEs (Fig. 5c). After 14 days, the efficiencies of the CuO CE based solar cells with the ruthenium dye were found to be statistically similar to each other. The findings of this study suggest that the type of CE has an important impact on the long-term stability of DSSCs. The electrochemical impedance spectroscopy (EIS) measurements of the DSSC devices using different CuO and Pt counter electrodes are shown in Fig. 5d. During the EIS characterization, the devices were under constant AM 1.5 G, 100 mW/cm² illumination. The active area of the cell size was kept 0.25 cm² and the impedance of the solar cell was investigated by applying a bias at the V_{OC} and using an AC amplitude of 10 mV. The frequency range of the impedance spectra was from 0.1 Hz to 100 kHz. The equivalent circuit model used to show the internal impedance of the DSSCs (inset Fig. 5d). The series resistance R_S is associated with the contribution from the FTO and CE. The resistance R_{CE} is associated with the impedance at the CE/electrolyte interface. The resistance R_{ct} is associated with the impedance at the photoanode/dye/electrolyte interface. WD (Warburg impedance) corresponds to the ion diffusion resistance of the electrolyte. EIS measurements show that the interface impedance of the Pt CE was larger than that of the CuO CE, indicating larger resistance due to lower distribution density of the Pt CE on substrate, which resulted in a larger electrical resistance and lower charge transfer impedance between the Pt CEs and electrolyte.

4 Conclusion

This study demonstrated the production of graphene–TiO₂ photoanode with CuO CE. The graphene/TiO₂ nanostructures as photoanodes exhibited a high surface area for increasing dye adsorption and perfect electrical and thermal conductivity. It was also shown that the CuO nanorods exhibited higher solar cell efficiency compared to the conventional Pt CE. The highest solar conversion efficiency of 6.18% was obtained by using CuO CE. The variation of EQE with wavelength for the hybrid structures was investigated by using CuO CE and it was found that CuO CE-based solar cells had highest quantum efficiency which can be attributed to good electrocatalytic activity and low sheet resistance. The results of this study provide a new and cost effective method to enhance the performance of DSSCs by using highly catalytic and earth abundant materials formed from CuO thin films.

References

- Anandan, S., Wen, X., Yang, S.: Room temperature growth of CuO nanorod arrays on copper and their application as a cathode in dye-sensitized solar cells. *Mater. Chem. Phys.* **93**(1), 35–40 (2005a)
- Anandan, S., Wen, X., Yang, S.: Room temperature growth of CuO nanorod arrays on copper and their application as a cathode in dye-sensitized solar cells. *Mater. Chem. Phys.* **93**, 35–40 (2005b)
- Chung, I., Lee, B., He, J., Chang, R.P., Kanatzidis, M.G.: All-solid-state dye-sensitized solar cells with high efficiency. *Nature* **485**(7399), 486–489 (2012)
- Dao, V.D., Larina, L.L., Suh, H., Hong, K., Lee, J.K., Choi, H.S.: Optimum strategy for designing a graphene-based counter electrode for dye-sensitized solar cells. *Carbon* **1**(77), 980–992 (2014)
- Dao, V.D., Larina, L.L., Tran, Q.C., Bui, V.T., Nguyen, V.T., Pham, T.D., Choi, H.S.: Evaluation of Pt-based alloy/graphene nanohybrid electrocatalysts for triiodide reduction in photovoltaics. *Carbon* **116**, 294–302 (2017)

- Favereau, L., Warnan, J., Pellegrin, Y., Blart, E., Boujtita, M., Jacquemin, D., Odobel, F.: Diketopyrrolopyrrole derivatives for efficient NiO-based dye-sensitized solar cells. *Chem. Commun.* **49**(73), 8018–8020 (2013)
- Feng, X., Shankar, K., Varghese, O.K., Paulose, M., Latempa, T.J., Grimes, C.A.: Vertically aligned single crystal TiO₂ nanowire arrays grown directly on transparent conducting oxide coated glass: synthesis details and applications. *Nano Lett.* **8**(11), 3781–3786 (2008)
- Golobostanfarid, M.R., Abdizadeh, H.: Hierarchical porous titania/carbon nanotube nanocomposite photoanode synthesized by controlled phase separation for dye sensitized solar cell. *Sol. Energy Mater. Sol. Cells* **31**(120), 295–302 (2014)
- Grätzel, M.: Dye-sensitized solar cells. *J. Photochem. Photobiol. C* **4**(2), 145–153 (2003)
- Hagfeldt, A., Boschloo, G., Sun, L., Kloo, L., Pettersson, H.: Dye-sensitized solar cells. *Chem. Rev.* **110**(11), 6595–6663 (2010)
- Kakiage, K., Aoyama, Y., Yano, T., Oya, K., Fujisawa, J.I., Hanaya, M.: Highly-efficient dye-sensitized solar cells with collaborative sensitization by silyl-anchor and carboxy-anchor dyes. *Chem. Commun.* **51**(88), 15894–15897 (2015)
- Le Pleux, L., Smeigh, A.L., Gibson, E., Pellegrin, Y., Blart, E., Boschloo, G., Hagfeldt, A., Hammarström, L., Odobel, F.: Synthesis, photophysical and photovoltaic investigations of acceptor-functionalized perylene monoimide dyes for nickel oxide p-type dye-sensitized solar cells. *Energy Environ. Sci.* **4**(6), 2075–2084 (2011)
- Liu, Y., Liao, L., Li, J., Pan, C.: From copper nanocrystalline to CuO nanoneedle array: synthesis, growth mechanism, and properties. *J. Phys. Chem. C* **111**, 5050–5056 (2007)
- Mathew, S., Yella, A., Gao, P., Humphry-Baker, R., Curchod, B.F., Ashari-Astani, N., Tavernelli, I., Rothlisberger, U., Nazeeruddin, M.K., Grätzel, M.: Dye-sensitized solar cells with 13% efficiency achieved through the molecular engineering of porphyrin sensitizers. *Nat. Chem.* **6**(3), 242–247 (2014)
- Morandira, A., Boschloo, G., Hagfeldt, A., Hammarstrom, L.: Coumarin 343—NiO films as nanostructured photocathodes in dye-sensitized solar cells: ultrafast electron transfer, effect of the I³⁻/I⁻ redox couple and mechanism of photocurrent generation. *J. Phys. Chem. C* **112**(25), 9530–9537 (2008)
- O’regan, B., Grätzel, M.: A low-cost, high-efficiency solar cell based on dye-sensitized colloidal TiO₂ films. *Nature* **353**(6346), 737–740 (1991)
- Odobel, F., Pellegrin, Y.: Recent advances in the sensitization of wide-band-gap nanostructured p-type semiconductors. Photovoltaic and photocatalytic applications. *J. Phys. Chem. Lett.* **4**(15), 2551–2564 (2013)
- Oh, H.J., Dao, V.D., Choi, H.S.: Cost-effective CoPd alloy/reduced graphene oxide counter electrodes as a new avenue for high-efficiency liquid junction photovoltaic devices. *J. Alloys Compd.* **705**, 610–617 (2017)
- Park, E., Lee, Y., Dao, V.D., Cam, N.T.D., Choi, H.S.: Design of CoNi alloy/graphene as an efficient Pt-free counter electrode in liquid junction photovoltaic devices. *Synth. Met.* **230**, 97–104 (2017)
- Poudel, P., Qiao, Q.: Carbon nanostructure counter electrodes for low cost and stable dye-sensitized solar cells. *Nano Energy* **31**(4), 157–175 (2014)
- Qin, P., Wiberg, J., Gibson, E.A., Linder, M., Li, L., Brinck, T., Hagfeldt, A., Albinsson, B., Sun, L.: Synthesis and mechanistic studies of organic chromophores with different energy levels for p-type dye-sensitized solar cells. *J. Phys. Chem. C* **114**(10), 4738–4748 (2010)
- Sharma, J.K., Akhtar, M.S., Ameen, S., Srivastava, P., Singh, G.: Green synthesis of CuO nanoparticles with leaf extract of *Calotropis gigantea* and its dye-sensitized solar cells applications. *J. Alloys Compd.* **632**, 321–325 (2015)
- Sim, E., Dao, V.D., Choi, H.S.: Pt-free counter electrode based on FeNi alloy/reduced graphene oxide in liquid junction photovoltaic devices. *J. Alloys Compd.* **742**, 334–341 (2018)
- Tsai, C.H., Fei, P.H., Lin, C.M., Shiu, S.L.: CuO and CuO/graphene nanostructured thin films as counter electrodes for Pt-free dye-sensitized solar cells. *Coatings* **8**(1), 21 (2018)
- Wang, X., Zhi, L., Müllen, K.: Transparent, conductive graphene electrodes for dye-sensitized solar cells. *Nano Lett.* **8**(1), 323–327 (2008)
- Wood, C.J., Cheng, M., Clark, C.A., Horvath, R., Clark, I.P., Hamilton, M.L., Towrie, M., George, M.W., Sun, L., Yang, X., Gibson, E.A.: Red-absorbing cationic acceptor dyes for photocathodes in tandem solar cells. *J. Phys. Chem. C* **118**(30), 16536–16546 (2014)
- Zhang, Q., Cao, G.: Hierarchically structured photoelectrodes for dye-sensitized solar cells. *J. Mater. Chem.* **21**(19), 6769–6774 (2011)